Selecting detection wavelength of resonant cavity-enhanced photodetectors by guided-mode resonance reflectors

Kuo-Wei Lai, Yi-Shan Lee, Ying-Jhe Fu, and Sheng-Di Lin*

Department of Electronics Engineering, National Chiao Tung University, 1001 University Road, Hsinchu 300, Taiwan

sdlin@mail.cntu.edu.tw

Abstract: We propose and demonstrate a novel device structure of resonant cavity-enhanced photodetector (RCE-PD). The new RCE-PD structure consists of a bottom distributed Bragg reflector (DBR), a cavity with InGaAs multiple quantum wells (MQWs) for light absorption and a top mirror of sub-wavelength grating. By changing the fill factor of the 2-D grating, the effective cavity length of RCE-PDs can be varied so the resonant wavelength can be selected post growth. Accordingly, we can fabricate an array of PDs on a single chip, on which every PD aims for a specific wavelength.

OCIS codes: (040.5160) Photodetectors; (230.1950) Diffraction gratings.

References and links

1. K. Kishino, M. S. Unlu, J. I. Chyi, J. Reed, L. Arsenault, and H. Morkoc, "Resonant cavity-enhanced (RCE) Photodetector," IEEE J. Quantum Electron. **27**(8), 2025–2034 (1991).
2. M. S. Ünlü and S. Strite, "Resonant cavity enhanced photonic devices," J. Appl. Phys. **78**(2), 607–639 (1995).
3. J. P. Kim and A. M. Sarangan, "Simulation of resonant cavity enhanced (RCE) photodetectors using the finite difference time domain (FDTD) method," Opt. Express **12**(20), 4829–4834 (2004).
4. S. S. Murtaza, I.-H. Tan, J. E. Bowers, E. L. Hu, K. A. Anselm, M. R. Islam, R. V. Chelakara, R. D. Dupuis, B. G. Streetman, and J. C. Campbell, "High-finesse resonant-cavity photodetectors with an adjustable resonance frequency," J. Lightwave Technol. **14**(6), 1081–1089 (1996).
5. E. Özbay, I. Kimukin, N. Biyikli, O. Aytur, M. Gokkavas, G. Ulu, M. S. Unlu, R. P. Mirin, K. A. Bertness, and D. H. Christensen, "High-speed >90% quantum-efficiency p–i–n photodiodes with a resonance wavelength adjustable in the 795–835 nm range," Appl. Phys. Lett. **74**(8), 1072–1074 (1999).
6. K. Lai and J. C. Campbell, "Design of a tunable GaAs/AlGaAs multiple-quantum-well resonant-cavity photodetector," IEEE J. Quantum Electron. **30**(1), 108–114 (1994).
7. Y. Shi, J. H. Zhao, J. Sarathy, H. Lee, and G. H. Olsen, "Tunable photodetectors based on strain compensated GaInAsSb/AlGaAsSb multiple quantum wells grown by molecular beam epitaxy," IEEE Trans. Electron. Dev. **44**(12), 2167–2173 (1997).
8. R. W. Mao, Y. H. Zuo, C. B. Li, B. W. Cheng, X. G. Teng, L. P. Luo, J. Z. Yu, and Q. M. Wang, "Demonstration of low-cost Si-based tunable long-wavelength resonant-cavity-enhanced photodetectors," Appl. Phys. Lett. **86**(3), 033502 (2005).
9. S. Foland, K. H. Choi, and J. B. Lee, "Pressure-tunable guided-mode resonance sensor for single-wavelength characterization," Opt. Lett. **35**(23), 3871–3873 (2010).
10. Y. Zhou, M. C. Y. Huang, and C. J. Chang-Hasnain, "Tunable VCSEL with ultra-thin high contrast grating for high-speed tuning," Opt. Express **16**(18), 14221–14226 (2008).
11. Y. Zhou, M. C. Y. Huang, C. Chase, V. Karagodsky, M. Moewe, B. Pesala, F. G. Sedgwick, and C. J. Chang-Hasnain, "High-index-contrast grating (HCG) and its applications in optoelectronic devices," IEEE J. Sel. Top. Quantum Electron. **15**(5), 1485–1499 (2009).
12. S. S. Wang, R. Magnusson, J. S. Bagby, and M. G. Moharam, "Guided-mode resonances in planar dielectric layer diffraction gratings," J. Opt. Soc. Am. A **7**(8), 1470–1474 (1990).
13. A. Sharon, D. Rosenblatt, and A. A. Friesem, "Resonant grating-waveguide structures for visible and near-infared radiation," J. Opt. Soc. Am. A **14**(11), 2985–2993 (1997).
14. C. F. R. Mateus, M. C. Y. Huang, Y. Deng, A. R. Neureuther, and C. J. Chang-Hasnain, "Ultrabroadband mirror using low-index cladded subwavelength grating," IEEE Photon. Technol. Lett. **16**(2), 518–520 (2004).
15. Y. S. Yang, Y. Q. Huang, X. M. Ren, X. A. Ye, X. F. Duan, H. Huang, and Q. Wang, "Design net-grid subwavelength gratings for high quantum efficiency photodetectors," Adv. Mater. Res. **93–94**, 43–48 (2010).
16. M. Zohar, M. Auslender, L. Faraone, and S. Hava, "Novel resonant cavity-enhanced absorber structures for high-efficiency mid-infrared photodetector application," J. Nanophoton. **5**(1), 051824 (2011).

#159696 - $15.00 USD Received 9 Dec 2011; revised 17 Jan 2012; accepted 18 Jan 2012; published 30 Jan 2012

17. V. Karagodsky, F. G. Sedgwick, and C. J. Chang-Hasnain, "Theoretical analysis of subwavelength high contrast grating reflectors," Opt. Express **18**(16), 16973–16988 (2010).
18. D. L. Brundrett, E. N. Glytsis, and T. K. Gaylord, "Homogeneous layer models for high-spatial-frequency dielectric surface-relief gratings: conical diffraction and antireflection designs," Appl. Opt. **33**(13), 2695–2706 (1994).
19. S. Peng and G. M. Morris, "Experimental demonstration of resonant anomalies in diffraction from two-dimensional gratings," Opt. Lett. **21**(8), 549–551 (1996).
20. M. G. Moharam and T. K. Gaylord, "Rigorous coupled-wave analysis of planar grating diffraction," J. Opt. Soc. Am. **71**(7), 811–818 (1981).
21. M. S. Alam, M. S. Rahman, M. R. Islam, A. G. Bhuiyan, and M. Yamada, "Refractive index, absorption coefficient, and photoelastic constant: key parameters of InGaAs material relevant to InGaAs-based device performance," in *IEEE 19th International Conference on Indium Phosphide & Related Materials, 2007. IPRM '07* (IEEE, 2007), pp. 343–346.
22. K. Kurihara, T. Numai, I. Ogura, A. Yasuda, M. Sugimoto, and K. Kasahara, "Reduction in the series resistance of the distributed Bragg reflector in vertical cavities by using quasigraded superlattices at the heterointerfaces," J. Appl. Phys. **73**(1), 21–27 (1993).
23. S. C. Huang, T. H. Yang, C. P. Lee, and S. D. Lin, "Electrically driven integrated photonic crystal nanocavity coupled surface emitting laser," Appl. Phys. Lett. **90**(15), 151121 (2007).

1. Introduction

Resonant cavity-enhanced photodetectors (RCE-PDs) have been studied for long because they offer the attractive advantages over conventional p-i-n photodetectors in terms of high-speed and high quantum efficiency [1–3]. In addition, the selectivity of detection wavelength of RCE-PDs reduces the cross talk between adjacent devices so they are suitable candidates for integrated opto-electronic system. Selecting or tuning of the resonant wavelength post growth is desirable in many applications such as optical communication and gas sensing, etc.. However, it is usually difficult to adjust the resonant wavelength after epitaxy growth. Enormous efforts have been put on tailoring the resonant wavelength and many methods have been developed. The recess etch of top layer is an easy way for tuning the resonant wavelength and a tuning range of 40 nm (795 - 835 nm) was achieved [4,5]. Electrical control through Stark's effect is superior because its resonant wavelength can be controlled even after the device processing [6,7]. However, these two methods need high absorption layers which may slow down the response speed of devices. Tuning with heating effect may be low-cost but the reported tuning range is only 15.4 nm [8]. Foland and his associates proposed that, by applying pressure on a 1-D grating mirror, the effective refractive index can be changed so the reflectivity peak can be adjusted [9]. Their tuning range is also very limited and has not been demonstrated experimentally. The electro-mechanical control is promising as it has been realized on vertical cavity surface emitting laser (VCSEL) [10]. On the other hand, the emerging of sub-wavelength grating attracts much attention due to its novel optical properties and flexibility in integrating with other devices [11–17]. With a single layer serving as a grating and also a waveguide, the sub-wavelength grating exhibits wide-band high-reflectivity based on the guided-mode resonance (GMR) effect. Benefiting from its much thinner thickness and flexibility during device processing, the reflector using GMR effect has been implemented in many photonic devices instead of conventional DBR mirror [11]. In this paper, we propose the use of GMR reflector as the top mirror of the RCE-PDs. As we shall present, this approach not only takes the advantage of much thinner thickness of GMR mirror, but also provides a new and easy method to select the resonant wavelength of RCE-PDs.

Because the cavity length is fixed after the sample growth, the resonant wavelength of conventional RCE-PDs with two DBRs is usually fixed. We propose a new structure of RCE-PDs consisting of a bottom DBR, a cavity with InGaAs multiple quantum wells (MQWs) for light absorption and a top GMR mirror, as shown in Fig. 1(a). The top DBR is replaced with a GMR reflector which is a suspended grating. With the well-designed GMR grating, we can select the definite absorption wavelength during device processing. The desired resonant wavelength can be adjusted by changing the fill factor of the 2-D square-lattice grating. Accordingly, we can fabricate an array of RCE-PDs on a single chip, on which every PD aims for a specific wavelength, which could be of great use in applications such as optical interconnect and miniature spectrometer.

#159696 - $15.00 USD Received 9 Dec 2011; revised 17 Jan 2012; accepted 18 Jan 2012; published 30 Jan 2012

2. Device design and simulation

2.1 Design concept

In the aspect of optical consideration, RCD-PDs consist of three parts, bottom mirror, cavity with absorption layer, and top mirror [1]. To maximize the detection efficiency, the reflectivity of bottom mirror has to be as high as possible, which is typically achieved with a DBR reflector. Regarding to the cavity layer, once the detection wavelength has been assigned, the thickness and materials can be decided accordingly. The reflectivity of the top mirror, however, has to be optimized based on the absorption of the cavity layer [1]. Usually smaller absorption needs higher reflectivity to obtain the optimized quantum efficiency. With a proper design, RCE-PDs can achieve nearly 100% quantum efficiency. However, regarding to the detection wavelength, RCE-PDs is usually narrow band and the resonant wavelength is fixed during sample growth or top mirror coating. Here we present a new type of RCE-PD shown in Fig. 1(a). In our structure, conventional bottom DBR mirror and a cavity with embedded InGaAs MQWs serving as absorption layers are used. The top mirror, however, is replaced with a suspending GMR reflector.

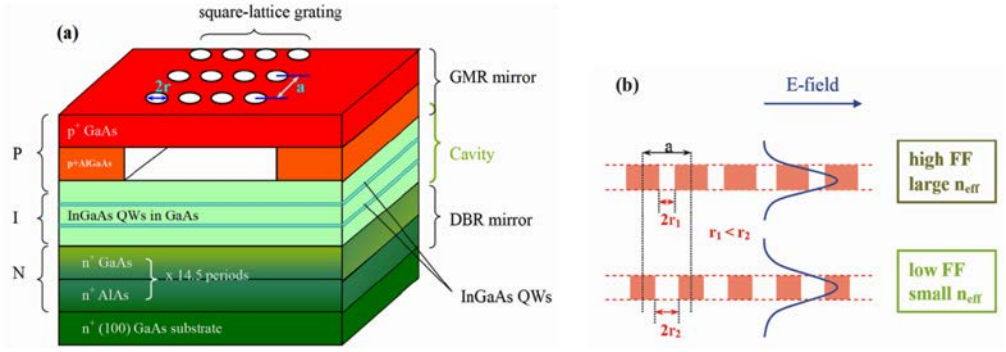

Fig. 1. The schematics of (a) a RCE-PD with a suspending GMR reflector, and (b) two GMR gratings with different effective refractive indexes and the corresponding guiding mode profiles.

GMR is a coupling effect between the grating diffraction and the guided mode [12, 13]. In single-layer GMR grating, the grating itself also serves as a waveguide layer. That is, as the diffracted rays couple into the guided mode of grating, a resonant condition can be met to make the reflected light interference constructively so nearly 100% reflectivity could be achieved [14]. Although GMR reflector of 1-D grating is studied extensively, we choose 2-D grating instead due to its ease of fabrication (exactly the fabrication of a conventional 2-D photonic crystal membrane). One obvious advantage of using GMR mirror is its much thinner thickness (~λ, the designed wavelength), comparing with that of a DBR reflector (~10λ). The other one, which is even more significant, comes from its adjustable effective refractive index. In the view of effective medium theory (EMT), the grating can be treated as a waveguide with an effective refractive index, n_{eff}. The n_{eff} depends on the fill factor (FF) of the 2-D grating, defined as $FF = 1-(\pi r^2/a^2)$ [18, 19]. The r and a are the hole radius and period of the grating, respectively. Because r and a are processing parameters, we can adjust the fill factor so as the effective refractive index n_{eff} during device fabrication. Different fill factor gives different n_{eff} so the guided mode profile can be modified. As illustrated in Fig. 1(b), with the same period *a*, smaller hole radius (r_1) gives higher FF and larger n_{eff}, resulting with a more confined mode profile. Putting this thought back into the RCE-PD in Fig. 1(a), the effective cavity length is affected by the mode profile of the GMR mirror so the resonant wavelength is adjustable simply by changing the hole radius r. That is, in our RCE-PDs with the well-designed grating parameter, a definite absorption wavelength can be selected during device processing. With this method, it becomes feasible to fabricate an array of RCE-PDs with wavelength selectivity on a single chip.

#159696 - $15.00 USD Received 9 Dec 2011; revised 17 Jan 2012; accepted 18 Jan 2012; published 30 Jan 2012

2.2 Simulation

To verify our design concept, a numerical simulation based on the method of rigorous coupled-wave analysis [20] is performed with the commercial software, DiffractMOD3.1, produced by RSoft Design Group. By inputting the structure parameters of thickness and refractive index of each material, the reflectivity/absorption/transmission spectra and steady-state electric field distribution can be calculated. The absorption coefficient of $In_{0.2}Ga_{0.8}As$ QW is set as 1 μm^{-1} [21] and the refractive index of GaAs (AlAs) is 3.54 (2.97). The broad-band top GMR reflector is made of a strong refractive-index-modulation grating consisting of GaAs and air, where the lowest diffraction and guided-mode orders are selected [12–14]. Square-lattice gratings (period a = 570 nm) and circular holes with various radius (r = 170 - 230 nm) are chosen for normal-incident polarization-insensitive application [19]. The GMR mirror itself has a reflectivity around 0.8 over a bandwidth of around 100 nm. The simulated absorption spectra of the designed structure with various fill factors are plotted in Fig. 2(a). As the fill factor (FF) decreases from 0.698 (curve 1) to 0.497 (curve 10), the corresponding absorption peaks blue shift from 968 nm to 923 nm. A span of 45 nm with full-with-half-maximum (FWHM) of 4-8 nm is obtained. We can see that the spectral linewidth is narrower when the absorption is higher, which is similar to the analysis in Refs. [1] and [4]. The highest absorption of 83% can be achieved with the fill factor of 0.522 (curve 9).

To understand the tuning behavior of fill factors, we plot the effective refractive index (n_{eff}) of the grating and resonant wavelength (λ_{res}) in Fig. 2(b). Note that, unlike the case of 1-D grating whose effective refractive index can be solved analytically [15], the n_{eff} of a 2-D grating is calculated by fitting its long wavelength (> 10 μm) reflection spectra to that of a uniform waveguide with refractive index n_{eff}. As shown in Fig. 2(b), with increasing filling factors FF, n_{eff} of the grating increases and λ_{res} red shifts. This can be understood in the following way. The cavity length is determined by the optical distance from the bottom of suspending grating to the interface between the cavity layer and the bottom DBR mirror. As sketched in Fig. 1(b), a grating with larger n_{eff} gives more confined field distribution inside the waveguide. In term of the phase of the electromagnetic (EM) wave, when optical thickness of a waveguide is less or around the wavelength under discussion, the waveguide with larger n_{eff} has an advancing phase at the air/dielectric interface comparing with the one with small n_{eff}. As a result, for the larger n_{eff} waveguide, the EM wave with longer wavelength can meet the resonance condition of the cavity because of the fixed boundary condition at the interface between the cavity layer and the bottom DBR mirror. This interpretation is also clearly revealed with the simulated electric field distribution plotted in Fig. 2(c). Note that the electric field distribution is plotted at the resonant wavelengths and only for the region near the cavity for clarity. As the fill factor (FF) decreases from 0.615 to 0.570, the effective refractive index n_{eff} decreases and the resonant wavelengths blue shift from 950 nm to 941 nm. The decreasing n_{eff} causes a wider mode profile which gives a delayed phase at the interface between the air and the grating. As a result, the peak of electric field in the air moves away from the grating so the resonant wavelength is shortened. Actually, as we can see in Fig. 2(c), the electric field distributions of the three wavelengths are nearly the same when the waves propagate into the GaAs and InGaAs QWs region. The alignment of InGaAs QWs and anti-nodes is not affected by the varied resonant wavelengths.

These simulated results demonstrate that, by changing the fill factor of the GMR grating, we can tune the resonant absorption wavelength of RCE-PDs with top GMR mirror. Note that the span is mainly limited by the grating processing because it is not practical to make a hole with too small (lithography limit) or too large radius (two adjacent holes touching each other). In addition, aside from the materials parameters, the tuning range also strongly depends on the cavity length (the total distance between the GMR grating and the DBR mirror). The largest theoretical tuning range achievable with our current structure is about 60 nm but a larger tuning may be possible if a different material system can be applied to.

#159696 - $15.00 USD Received 9 Dec 2011; revised 17 Jan 2012; accepted 18 Jan 2012; published 30 Jan 2012

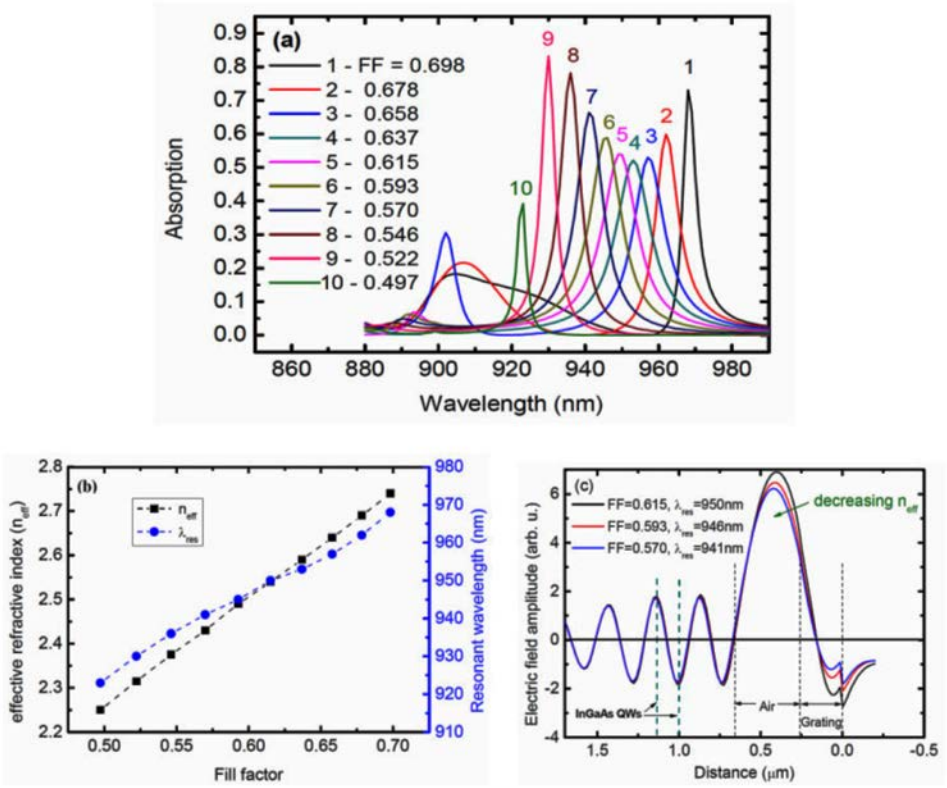

Fig. 2. Simulation results from the designed RCE-PD structure with various fill factors: (a) the absorption spectra, and (b) the resonant wavelength and the effective refractive index, and (c) simulated electric field distribution at the resonant wavelengths for FF = 0.615, 0.593 and 0.570.

3. Sample growth, device fabrication and measurement method

The sample (RN0979) was grown on (100) n^+-GaAs substrate by a solid-source molecular beam epitaxy (MBE) system. The sample structure illustrated in Fig. 3, including the bottom DBR, the cavity and the GMR layers, is detailed here. Firstly, the n-typed bottom DBR is composed of 14.5 periods λ/4 GaAs/AlAs layers. At the GaAl/AlAs interface, a digitally-graded and highly-doped superlattice (lower-left panel in Fig. 3) is inserted to lower the series resistance caused by the band discontinuity [22]. Secondly, the cavity layer above the bottom DBR is formed with 10-nm-thick $In_{0.2}Ga_{0.8}As$ MQWs in undoped GaAs matrix. A p^+-GaAs layer (213 nm, $p^+ = 1x10^{19}$ cm^{-3}) is added on the top of undoped GaAs for lateral current conduction (lower-central panel in Fig. 3). Note that, to maximize the absorption efficiency, the four InGaAs QWs are placed at the two anti-nodes of electric field obtained from the simulation (top panel in Fig. 3). Finally, the sample growth ends with the GMR mirror layer. The 400-nm p^+-$Al_{0.8}Ga_{0.2}As$ serves as the sacrificing layer to form the suspending GMR grating afterward. The grating is made from the top 280-nm p^+-GaAs contact layer by subsequent e-beam lithography and dry etch (lower-right panel in Fig. 3). By characterizing the etched sample, the graded DBR exhibits a reflectivity higher than 95% in 925 - 980 nm and the peak of photoluminescence spectra of InGaAs MQWs is around 990 nm.

The fabrication of the RCE-PD with GMR mirror is basically consisting of two processes: making a suspending 2-D grating (the same as making a photonic crystal) and a standard process of p-i-n photodiodes with top optical window. We start with the grating processing, including hard mask deposition (PECVD SiN_x, 400 nm), e-beam lithography of the grating, pattern transferring to SiN_x then to GaAs through inductive-coupled-plasma (ICP) dry etch.

#159696 - $15.00 USD Received 9 Dec 2011; revised 17 Jan 2012; accepted 18 Jan 2012; published 30 Jan 2012

Next, to define the device size of p-i-n photodiode, the mesa of 440 x 230 μm^2 down to the undoped GaAs layer is formed with chemical wet etch using the solution of H_2SO_4: H_2O_2: H_2O = 1: 8: 80. Ti/Au and Ni/Ge/Au multilayer metals are e-gun evaporated as p- and n-typed ohmic contacts, respectively, by conventional technique including standard photolithography, e-gun evaporation and lift-off. The size of optical window is 100 x 100 μm^2. The suspending GMR reflector is subsequently freed by removing the $Al_{0.8}Ga_{0.2}As$ sacrificing layer with diluted HF (HF: H_2O = 1: 25) while the area outside the optical window is protected with photoresist. The device processing is ended with rapid thermal annealing of ohmic contacts (420 °C / 35 s) in forming gases. To perform electrical and optical measurements, the chip is put on lead-free chip carrier and the devices are bonded with gold wire.

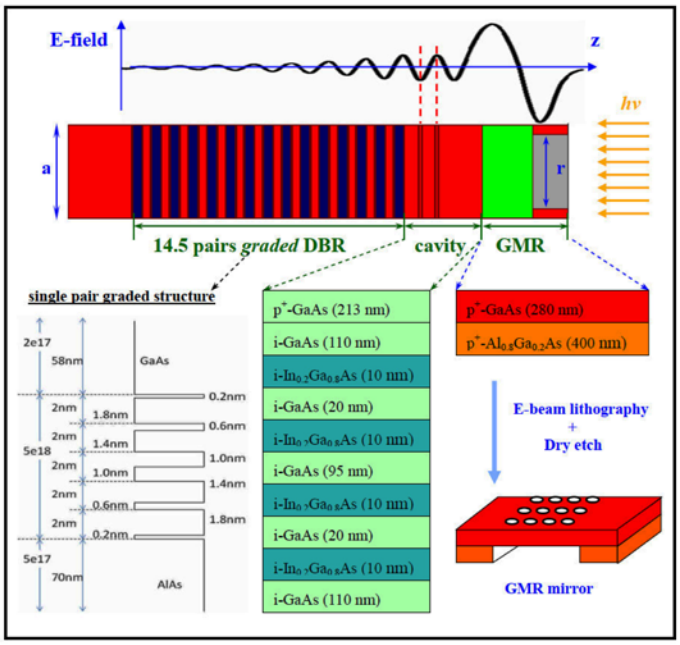

Fig. 3. The unit cell of the sample structure (middle panel), its corresponding electric field distribution (upper panel) and the detailed epitaxy structure (lower panel).

The dark current-voltage (I-V) curves of devices are measured with the semiconductor parameter analyzer HP 4145. To obtain relative responsivity spectra, we use the system of Fourier transform infrared spectroscopy (FTIR, Nicolet 6700) combined with the current pre-amplifier (Standford Research SR570). The photocurrent of the device illuminated by a white light source of FTIR is first amplified by the current pre-amplifier and then sent back to FTIR for signal processing. The absolute responsivity is calibrated with an 850-nm diode laser pigtailed with a bare fiber. The packaged device allows us to measure the responsivity spectra at various temperatures by attaching it onto the cold head of close-cycle cryostat.

4. Results and discussions

Figure 4 shows the measured responsivity spectra of the device with FF = 0.595. In Fig. 4(a), the SEM image of a part of the GMR grating and the dark I-V curve are also inserted. The turn-on voltage is around 1 V and the reverse current is less than 1 μA up to −3 V. For the responsivity spectra taken at 0 V, a clear peak at 951 nm due to resonant absorption in InGaAs MQWs is observed. The peak responsivity at 951 nm is about 0.18 A/W corresponding to an external quantum efficiency of 23%. There are three additional peaks around 900 nm, 981 nm and 1002 nm. Comparing with the spectra taken at – 3 V, we conclude that the peaks at 981 nm and 1002 nm arise from the excitonic absorption of InGaAs QWs because they are weaken by the applied electric field. The sudden rise around 870 nm is

#159696 - $15.00 USD Received 9 Dec 2011; revised 17 Jan 2012; accepted 18 Jan 2012; published 30 Jan 2012

caused by bulk GaAs absorption and the peak at 900 nm is due to the absorption of no-grating region. This assignment of the peaks can be further confirmed with the data in Fig. 4(b), the responsivity spectra measured at various temperatures. Although, as expected, all the peaks of the spectra blue shift with decreasing temperature, the shift rates are quite different among them. The peak at 951 nm, which we attribute to the designed resonant absorption, shifts much slower than the excitonic peak at 981 nm and 1002 nm. With increasing temperature, the excitonic peaks red shift due to the bandgap shrinkage effect. However, the shift of cavity resonant wavelength is decided by the change of refractive index with temperature, which is much weaker than bandgap shrinkage. By linearly fitting the peaks dependence on temperature, we found the peak shift rates of 0.09 nm / °C for 951-nm peak and 0.28 nm / °C for 981-nm and 1002-nm peaks, which is consistent with the previous study [23]. This also demonstrates that the detection wavelength of our devices is temperature-insensitive.

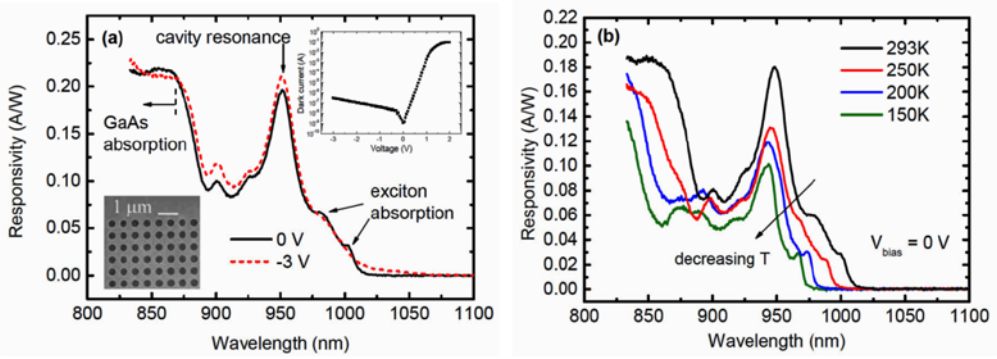

Fig. 4. The responsivity spectra of the device with FF = 0.595. (a) Taken at 0 V and –3 V at room temperature. Insets: the SEM picture of partial GMR grating (left) and the dark I-V curve (right). (b) Responsivity spectra measured at various temperatures.

As the resonant peaks can be tuned with the fill factor of grating, we can process many devices with various hole sizes on one chip. In Fig. 5(a), we show the responsivity spectra of four devices on the same chip. Note that the curves are vertically shifted for clarity. The resonant peaks shift from 946 nm to 954 nm when the fill factors are increased from 0.545 to 0.619. It is worth mentioning that the peak responsivities are nearly unchanged. It demonstrates that our method has the potential to fabricate an array of wavelength-sensitive photodetectors. In Fig. 5(b), we plot the experimental data together with the simulation results. For the resonant wavelength, there is a satisfying consistence between experiment and theory. However, for the FWHM, the measured linewidths of all devices are considerably larger than the simulated ones. By examining the epitaxy/processing parameters and temperature-dependence of responsivity spectra and with the help of simulation, we suspect

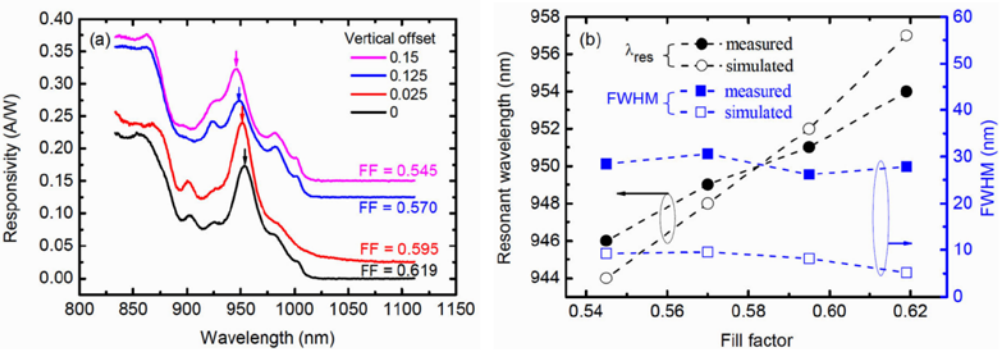

Fig. 5. The experimental responsivity spectra of four devices with different fill factors (a), and the measured and simulated resonant wavelengths and FWHMs (b).

#159696 - $15.00 USD Received 9 Dec 2011; revised 17 Jan 2012; accepted 18 Jan 2012; published 30 Jan 2012

that the discrepancy is mainly because of the surface/interface roughness of the GMR mirror. The roughness (~17 nm from atomic-force-microscopy measurement) caused by imperfect MBE epitaxy lowers the reflectivity of GMR reflector. As discussed in Ref. [1], the FWHM of the resonant peak can be considerably widened when the reflectivity of the top mirror is reduced. Other factors from epitaxy and/or processing could also play a role here but further investigations are needed to address this issue.

5. Conclusion

We presented the theoretical and experimental results of a novel RCE-PDs using GMR effect as the top mirror. The resonant wavelength can be selected simply by adjusting the fill factor of the GMR grating. Our work pave the way to realize the wavelength-sensitive photodetector array on a single chip, which may be of great use in various applications such as optical interconnect and miniature spectrometer.

Acknowledgments

This work was financially supported by the National Science Council and by the ATU Program of Ministry of Education in Taiwan. We thank the Center of Nano Science and Technology at National Chiao Tung University for their equipment support and Dr. Gray Lin for his helpful discussions. Preliminary work done by Mr. B. Y. Chou is highly appreciated.

#159696 - $15.00 USD Received 9 Dec 2011; revised 17 Jan 2012; accepted 18 Jan 2012; published 30 Jan 2012